Design of heterogeneous multicore fibers as sampled true-time delay lines

Sergi Garcia and Ivana Gasulla*

ITEAM Research Institute, Universitat Politecnica de Valencia, Camino de Vera s/n, Valencia 46022, Spain
**Corresponding author: ivgames@iteam.upv.es*

Received December 4, 2014; revised January 4, 2015; accepted January 7, 2015;
posted January 9, 2015 (Doc. ID 228886); published February 11, 2015

We present a novel procedure for designing a sampled discrete true-time delay line (TTDL) for Microwave Photonics applications based on a heterogeneous MCF. Both simple step-index (SI) and trench-assisted SI profiles are numerically evaluated in terms of physical dimensions and material dopant concentrations in order to individually tailor the group delay and chromatic dispersion of each core. The proposed TTDL features unique properties beyond the current state of the art in terms of record bandwidth, compactness, flexibility, and versatility. © 2015 Optical Society of America

OCIS codes: (060.2330) Fiber optics communications; (060.2360) Fiber optics links and subsystems; (060.5625) Radio frequency photonics; (350.4010) Microwaves.
http://dx.doi.org/10.1364/OL.40.000621

Microwave Photonics (MWP) brings numerous advantages to the generation, processing, and distribution of microwave and millimeter signals, not only those inherent to photonics engineering, but also key features such as fast tunability and reconfigurability that are not possible using classic electronic approaches. These attractive properties are behind the intense research activity on a wide range of information and communication solutions, including microwave signal filtering, optical beamforming for phase-array antennas, arbitrary waveform generation, and multigigabit per second analog-to-digital conversion [1]. Most of these approaches rely on a core optical component: the true time-delay line (TTDL). Different approaches have been reported for the implementation of this essential device, including switched and dispersive single-mode fibers, photonic crystal structures exploiting slow and fast light effects [2], active semiconductor waveguides based on quantum-dots [3], and nonlinear effects in optical fibers [4].

Despite the aforementioned application potential, the widespread adoption of MWP is still limited by the noncompact, heavy, and power-consuming nature of its up-to-date systems, in both signal processing and radio-over-fiber distribution scenarios. Integrated MWP has been proposed as a solution for the first scenario, but there is still a paramount need for a compact and efficient fiber-based technology able to support the required parallelization in distribution networks. This second scenario, which includes applications such as wireless access networks and fiber-to-the-home, usually resorts to the brute-force replication of a basic subsystem where the TTDL is built from discrete and bulky components. To solve these limitations and reduce the associated cost impact, we have proposed in [5] the extension of the concept of space-division multiplexing (SDM), currently restricted to high-capacity digital communications, to the area of MWP. More specifically, by exploitation of the inherent parallelism of heterogeneous multicore fibers (MCF), we envisioned the implementation of a sampled discrete TTDL featuring 2D (i.e., 2-dimensional) tunability.

Most of the research activity on SDM has employed the so-called homogeneous multicore fiber, where N identical single-mode cores are confined inside a single cladding with an outer diameter ranging from 150 to 200 μm. In order to increase the core packing density, heterogeneous MCF were later proposed. These are composed of nonidentical cores arranged so that the intercore crosstalk becomes sufficiently small as the phase matching condition is prevented [6]. State-of-the-art heterogeneous MCFs are composed of 2 or more different interleaved triangular lattices of homogeneous cores. Initial designs featured a crosstalk level below −30 dB at a length of 100 km when using 3 different core compositions in a standard 125-μm-diameter cladding [6]. High core densities were achieved when resorting to high values of the refractive index contrast ($\Delta = 1.15\%$, 1.20%, and 1.25%) in a 19-core fiber characterized by a pitch $\Lambda = 23$ μm and a core radius $a = 2.5$ μm [6]. Kokubun and Watanabe [7] found that a double-cladding structure can keep nearly identical the propagation characteristics of the cores, while accommodating up to 9 different equivalent refractive indexes in a 19-core fiber. Further progress in crosstalk management has been achieved by designing heterogeneous trench-assisted core configurations, where crosstalk levels lower than −40 dB for a 100-km link [8] have been obtained. While keeping comparable propagation characteristics in all the cores is important in digital communications, tunable TTDLs for MWP require different group delay and dispersion properties in each core. Here we present a new procedure for designing heterogeneous MCFs where one can tailor the chromatic dispersion parameter D of each core independently, assuring a low inter-core crosstalk. Typically, a tunable TTDL allows 1D (i.e., 1-dimensional) operation by exploiting optical wavelength diversity, using for example an array of lasers at different wavelengths. Our proposed TTDL adds more versatility, offering unprecedented 2D operation by also exploiting diversity in space, as shown in Fig. 1. This requires the design of an independent group delay $\tau(\lambda)$ per core, as shown in Figs. 2(c) and 2(d), according to an incremental law where the basic delay between cores $\Delta\tau$ depends on a common incremental dispersion parameter ΔD.

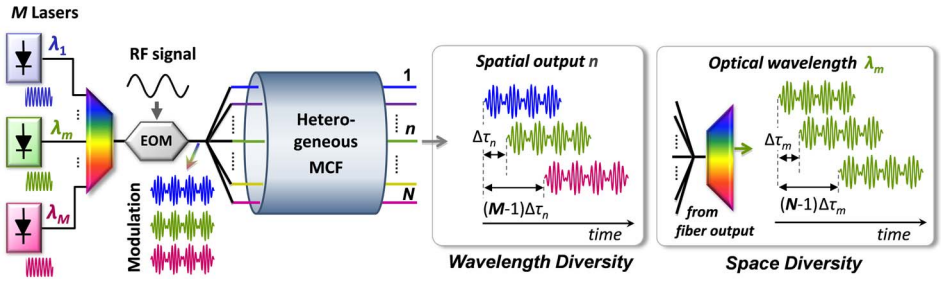

Fig. 1. 2D sampled TTDL fed by a RF-modulated multiple optical carrier.

By suitable modifications of material and waveguide dispersion, the group delay per unit length of the cores must be tailored according to the incremental law [5]:

$$\tau_n(\lambda) = \tau_o + [D_1 + (n-1)\Delta D](\lambda_m - \lambda_o), \quad (1)$$

where $n = 1, 2, \ldots N$ is the core number, τ_o is a basic group delay common to all cores for a given anchor or reference wavelength λ_o, λ_m is the operation wavelength, D_1 is the chromatic dispersion parameter for core 1, and ΔD is the incremental dispersion parameter between cores. When operating in space diversity, the basic differential group delay between adjacent cores, for a particular input wavelength λ_m, is given by

$$\Delta\tau_m(\lambda) = \Delta D(\lambda_m - \lambda_o), \quad \text{for } m = 1, 2, \ldots M, \quad (2)$$

as depicted in Fig. 2(c). Within a given core n, the use of wavelength diversity yields a basic differential group delay between adjacent wavelengths given by:

$$\Delta\tau_n = [D_1 + (n-1)\Delta D]\Delta\lambda, \quad \text{for } n = 1, 2, \ldots N, \quad (3)$$

being $\Delta\lambda$ the difference between 2 adjacent input optical wavelengths, as shown in Fig. 2(d).

The design of the heterogeneous MCF was carried out by means of a full vector finite-element method implemented using the Photon Design FIMMWAVE software that, so far, provides the most accurate solution for arbitrarily shaped waveguides with curved boundaries. We have designed the cross-section of the MCF assuming a negligible intercore crosstalk level, so that the dispersion profile of each core can been tailored individually. The numerical solver provides both the dispersion parameter D and the group refractive index n_g for a particular wavelength. Two different MCF structures have been considered: in the first each core presents a different refractive step-index (SI) profile surrounded by the cladding; in the second, the refractive index profile of each core is surrounded by a different trench, as depicted in Fig. 2(b). Since all the cores must share the same common group delay τ_o, we must design the refractive index profile of each core so that we obtain the same n_g at λ_o. In addition, we must assure an incremental value of the dispersion D following the law $D_n = D_1 + (n-1)\Delta D$. For the design of both models, we consider the same TTDL requirements: 7-sample operation characterized by $\Delta D = 1$ ps/(km · nm), that is, a dispersion range from 1 up to 7 ps/(km · nm).

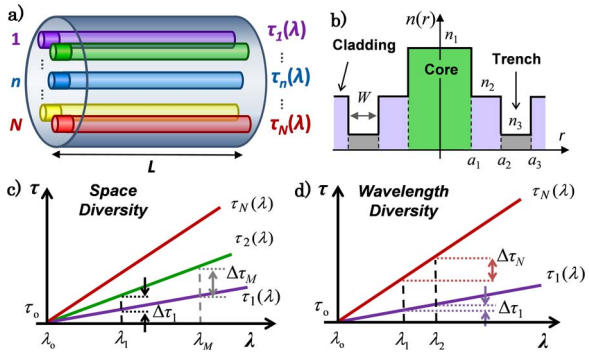

Fig. 2. (a) Heterogeneous MCF. (b) Trench-assisted SI profile. 2D TTDL operation: (c) space and (d) wavelength diversities.

The design of the dispersion profile of the first core model is linked to the selection of two design variables: the core radius a_1 and the fraction of GeO_2-dopant (mol. %) in the SiO_2 core. We first evaluated the dependence of n_g and D variables in the extended range of $2 \le a_1 \le 5$ μm and $1 \le GeO_2 \le 20$ mol. % at $\lambda_o = 1520$ nm. We then refined the range of GeO_2 dopant that offers a set of D parameters wide enough to tailor the required group delay slopes [from Eq. (1)]. Particularizing for a 7-core fiber, the selection of a common $n_g = 1.467$ assures the target dispersion ranging from 1 up to 7 ps/(km · nm). This is achieved for a GeO_2-dopant concentration bounded between 3.8 and 4.9 mol. %. The selected n_g results in a common group delay per unit length $\tau_o = n_g(\lambda_o)/c = 4.89$ ns/m, being c the speed of light in free space and $\lambda_o = 1520$ nm. Figure 3 shows the numerical computation of n_g and D as a function of the GeO_2 dopant for each designed core. The radius a_1 of each core has been set to match our dispersion requirements. The computed design parameters for this SI profile, which are depicted in rounded markers in Fig. 3, are summarized in Table 1. One can observe that an increase in the core GeO_2 concentration results in a linear increment of n_g and in a decrement of D. Taking into account that the core radius a_1 increases with the core number n, (as shown in Table 1), we can conclude that an increase in a_1 causes an increase in both n_g and D.

The second model, based on a trench-assisted refractive-index profile [as shown in Fig. 2(b)], allows a more versatile design. Apart from the core radius a_1 and the fraction of core dopant, the additional design parameters that can be changed are the internal and external radii of the trench, a_2 and a_3, and the amount of dopant in the trench. In order to achieve the required refractive index decrease in the trench (n_3) with respect to the cladding (n_2), we chose to dope all the core, cladding, and trench SiO_2 zones with different GeO_2 concentrations: from 10 to 15 mol. % for the core, a fixed 7.5 mol. % for the cladding, and from 0 to 5 mol. % for the trench. This low-index

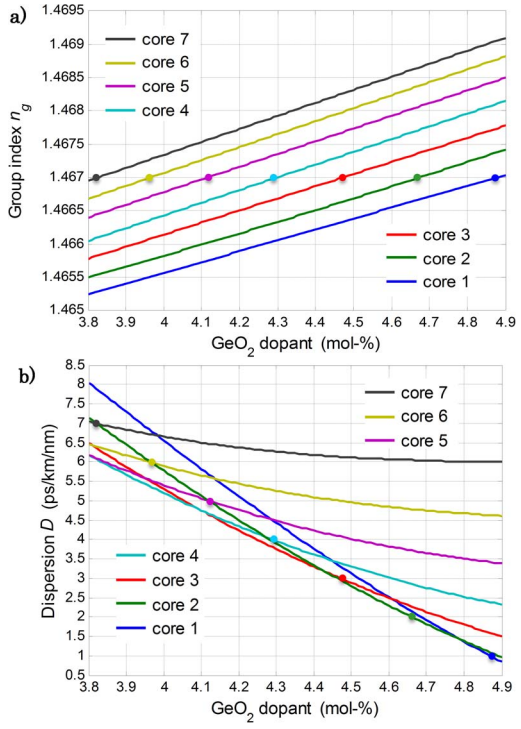

Fig. 3. Group index n_g (a) and Dispersion D (b) for the SI profile as a function of the core GeO_2 dopant percentage.

trench could also be implemented using a fluorine dopant (usually from 1 to 2 mol. %) [9]. As in the first model, we first evaluated the response of n_g and D for the mentioned GeO_2 percentages while varying the design radii as $2 \le a_1 \le 5$ μm, $0 \le a_2 - a_1 \le 2$ μm, and $1 \le a_3 - a_2 - a_1 \le 2$ μm. This coarse evaluation allowed us to refine the range of the five design variables that must assure, again, a set of D parameters wide enough to tailor the group delay slopes targeted for the 7-sample TTDL.

Figure 4 shows the dependence of n_g with the GeO_2 dopant of each core (from 11 to 12.5 mol. %, lower axis, solid lines), and with the GeO_2 dopant of their surrounding trenches (from 0 to 5 mol. %, upper axis, dashed lines). The dependence of the dispersion D with the proportion of GeO_2 in each core and trench can be seen, respectively, in Figs. 5(a) and 5(b). The selected values are indicated in rounded markers. The rest of the design variables remain, in each case, as shown in Table 1.

The core design, which involves both the GeO_2 concentration and radius a_1, plays the most important role in establishing the refined range for n_g and D. As seen

Table 1. Design Parameters for Each Core n in Both Models

Core	SI Profile		Trench-Assisted SI Profile				
n	a_1 (μm)	n_1 GeO_2 (mol. %)	a_1 (μm)	$a_2 - a_1$ (μm)	$a_3 - a_2$ $-a_1$ (μm)	n_1 GeO_2 (mol. %)	n_3 GeO_2 (mol. %)
1	2.075	4.87	2.850	1.200	1.650	11.50	0.00
2	2.150	4.66	3.000	1.050	1.390	11.50	0.00
3	2.270	4.47	3.000	1.120	1.370	11.50	0.00
4	2.370	4.29	3.000	1.000	1.180	12.00	5.00
5	2.477	4.12	2.900	1.720	1.000	12.00	3.61
6	2.590	3.96	3.040	1.510	1.000	12.00	5.00
7	2.715	3.82	3.250	1.000	1.250	11.60	5.00

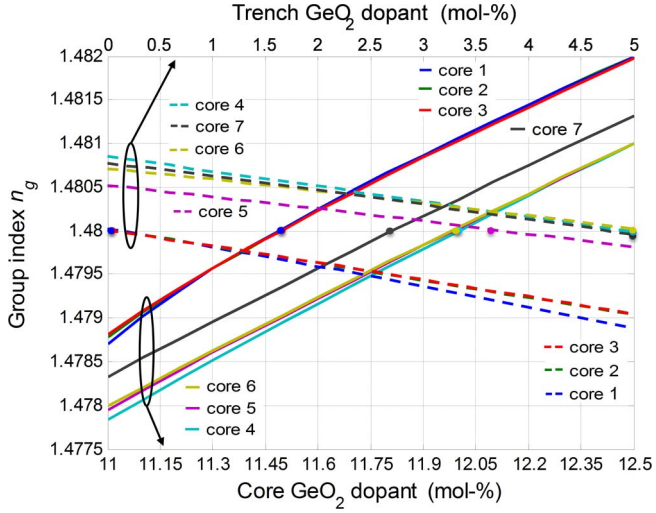

Fig. 4. Group index n_g for the trench-assisted profile as a function of the GeO_2 dopant percentage of the core (solid lines, lower axis) and the trench (dashed lines, upper axis).

in Fig. 4, n_g increases with the fraction of core GeO_2 dopant and also with the core radius a_1 (as stated before, a_1 increases with the core number n), while it decreases when the trench dopant increases. We have chosen $n_g = 1.480$ for $\lambda_o = 1520$ nm, which leads to a common group delay per unit length $\tau_o = 4.93$ ns/m. The same opposite sign slope behavior is illustrated in Fig. 5 for the dispersion. We can see in Fig. 5(a) that D increases substantially with the core GeO_2 doping percentage, while

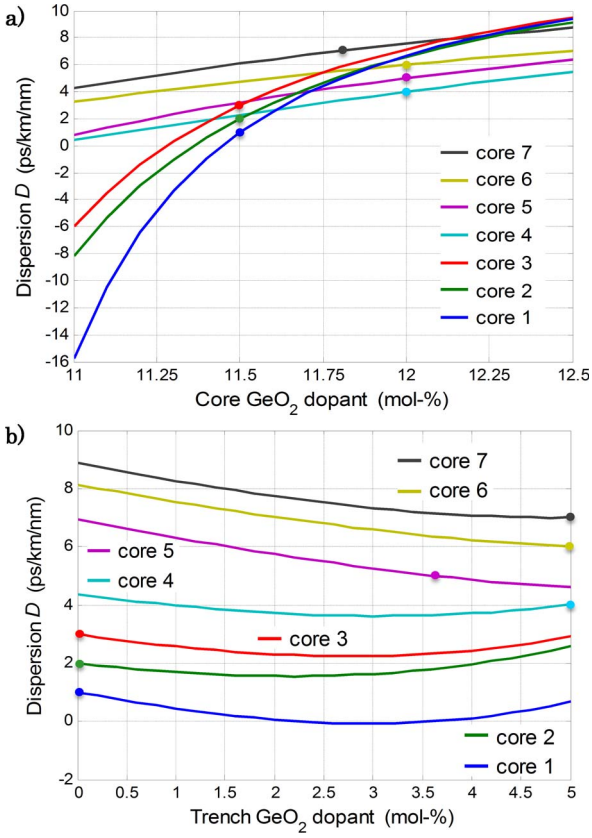

Fig. 5. Dispersion D for the trench-assisted profile as a function of the GeO_2 dopant of the core (a) and the trench (b).

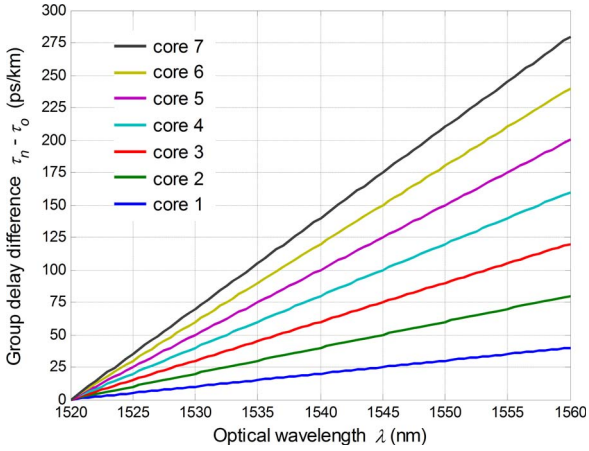

Fig. 6. Group delay difference $\tau_n(\lambda) - \tau_o$ per unit length versus the optical wavelength for each core.

Fig. 5(b) shows that it decreases with the increment in the trench dopant concentration and the core radius a_1.

Finally, we have evaluated the dependence of n_g and D with the geometrical properties of the trench. Although not illustrated here, it must be noted that the magnitude of n_g and D slightly decrease with an increase of the internal trench radius a_2, when keeping the rest of variables fixed. We also observed a linear increment in both parameters when increasing the trench width $(a_3 - a_2 - a_1)$ from 1 to 2 μm.

Once we have individually tailored the refractive index profile of each core in the two MCF models considered, we can evaluate the group delay dependence on the optical wavelength of the overall TTDL. Since both designs have the same number of cores and the same incremental dispersion parameter, they feature the same group delay slopes. Figure 6 shows these slopes (per unit length) calculated from Eq. (1) as the difference $\tau_n(\lambda) - \tau_o$ for a wavelength range up to 1560 nm.

The simultaneous exploitation of the space and wavelength diversity domains in the implemented 2D sampled TTDL adds more versatility as compared to current approaches where only wavelength diversity is exploited [4–7]. If we feed the 7-sample TTDL designed in this Letter by an array of $M = 10$ lasers (with $\Delta\lambda = 1$ nm), we obtain a basic differential delay range spanning from $\Delta\tau_1 = 1$ to $\Delta\tau_7 = 7$ ps/km when exploiting the wavelength diversity [Eq. (3)], while spanning from $\Delta\tau_1 = 1$ to $\Delta\tau_{10} = 10$ ps/km when using diversity in space [Eq. (2)]. These basic differential delays correspond to the possibility of sampling signal bandwidths ranging from 100 $GHz \cdot km$ to 1 $THz \cdot km$. For a 10-km MCF, these values yield a record frequency processing range spanning from 10 to 100 GHz, covering part of the X band, the Ku, K, Ka, V bands and part of the W band. A decrease in the MCF length down to 5 km will extend the frequency range from 20 up to 200 GHz, which will also include part of the millimeter band (110–300 GHz). The former bands embrace the vast majority of present and future MWP applications.

The numerical solver allows in addition to model the field propagation along the MCF length while applying different fiber curvatures. Both MCFs were designed with a cladding diameter of 125 μm and a core pitch $\Lambda = 40$ μm. The computation of the intercore crosstalk as a function of the bending radius provided a mean level of −50 dB for the SI profiles and −70 dB for the trench-assisted SI profiles. These levels, which are reached for radii larger than a critical bending radius of 50 mm, are lower than the −40 dB reached in state-of-the-art trench-assisted heterogeneous MCFs [8]. This is justified by the fact that the proposed TTDLs span fiber lengths (1–10 km) are lower than those required for high-capacity digital communications [6–8], and also from the fact that phase matching conditions are further prevented by the dissimilar cores.

We have proposed, for the first time to our knowledge, a novel method for the design of a sampled TTDL implemented with a heterogeneous MCF, where each core is characterized by a different group delay and dispersion profile. By properly tailoring the relevant variables of each core, we have obtained the required equally-spaced incremental group delay slopes. Two different MCF structures (one composed of simple SI-profiles and another one composed of trench-assisted SI profiles) have been considered for designing a TTDL with the same characteristics (number of samples and basic differential group delays). Apart from offering more flexibility throughout the design algorithm, the trench-assisted configuration assures a lower level of crosstalk and more robustness against fiber curvatures. This comes with the price of further complexity in the fabrication process. The proposed 2D TTDL features unique properties beyond the current state of the art in terms of record bandwidth, compactness, flexibility, and versatility. This will, in consequence has a positive impact on the final cost of MWP signal generation, processing, and distribution scenarios that are built upon a sampled TTDL.

The authors wish to acknowledge the financial support given by the Research Excellency Award Program GVA PROMETEO II/2013/012.

References

1. J. Capmany, J. Mora, I. Gasulla, J. Sancho, J. Lloret, and S. Sales, J. Lightwave Technol. **31**, 571 (2013).
2. J. Sancho, J. Bourderionnet, J. Lloret, S. Combrié, I. Gasulla, S. Xavier, S. Sales, P. Colman, G. Lehoucq, D. Dolfi, J. Capmany, and A. De Rossi, Nat. Commun. **3**, 1075 (2012).
3. F. Ohman, K. Yvind, and J. Mørk, Photon. Technol. Lett. **19**, 1145 (2007).
4. P. A. Morton and J. B. Khurgin, Photon. Technol. Lett. **21**, 1686 (2009).
5. I. Gasulla and J. Capmany, IEEE Photon. J. **4**, 877 (2012).
6. M. Koshiba, K. Saitoh, and Y. Kokubun, Electron. Express **6**, 98 (2009).
7. Y. Kokubun and T. Watanabe, in *Proceedings of IEEE Microoptics Conference (MOC)* (IEEE, 2011), p. K-5.
8. J. Tu, K. Saitoh, M. Koshiba, K. Takenaga, and S. Matsuo, Opt. Express **20**, 15157 (2012).
9. P. Watekar, S. Ju, and W. Han, Opt. Express **17**, 10350 (2009).